Computational physics with particles

Wm. G. Hoover and Carol G. Hoover
Ruby Valley Research Institute, Highway Contract 60, Box 598, Ruby Valley 89833, Nevada

(Received 31 July 2007; accepted 8 December 2007)

Microscopic and macroscopic particle simulation techniques are useful introductions to computational physics. These techniques make it possible to simulate complex problems in fluid and solid mechanics, including laminar and turbulent flows, shockwaves, as well as fracture and failure in solids. We illustrate several particle-based techniques with several examples. © *2008 American Association of Physics Teachers.*

[DOI: 10.1119/1.2830538]

I. INTRODUCTION

Because mesh-based finite-element techniques involve complex geometry and are prone to numerical instabilities, simulations of material flows are simplest using particles.[1–4] Particles move according to ordinary differential equations, which are relatively simple to formulate and to solve. From the atomistic viewpoint it is natural to use particles. Typical atomistic particles attract one another at long range and repel at short range. Gases, liquids, and solids can all be described by particle models of this kind. This computational particle description is called molecular dynamics, and originated about 50 years ago at the Los Alamos, Livermore, and Brookhaven National Laboratories.[5–9] The computational requirement is to solve the particle equations of motion,

$$m\ddot{r} = m\dot{v} = F_{\text{atomistic}} + F_{\text{boundary}} + F_{\text{constraints}} + F_{\text{driving}}, \quad (1)$$

where the boundary, constraint, and driving forces are used to control the motion of the atoms.

A solution of these equations gives the history of the coordinates $r(t)$ and velocities $v(t)$ which together give the state of the system. Because the additional forces (boundary, constraint, and driving) typically involve non-Hamiltonian dissipation, the usual symplectic integrators appropriate to Hamiltonian mechanics cannot be used for these problems. Numerical solutions of the first-order [in (d/dt)] ordinary differential equations of motion are most simply obtained by applying the Runge-Kutta method. The fourth-order Runge-Kutta method and its Fortran language implementation is given in Ref. 2, Sec. 1.6 and can be freely downloaded.[4] The Fortran and the equivalent C language implementations can be found in Ref. 3, Sec. 4.4. The full set of equations can conveniently be thought of as a single first-order equation describing the motion of a vector in the state space of the system.

The World War II computers which first made solving these equations possible were limited to just a few dozen particles. With increasing computer speeds simulations with millions or even billions of particles are possible today.[7,8] Such particle simulations can be a powerful aid to understanding material behavior. Watching the atomistic details of a melting crystal,[10] the formation of convection rolls in a heated fluid,[11] the development of shockwaves[12] and phase interfaces[13] provides a powerful incentive to understand macroscopic behavior in terms of microscopic models. The combination of computation with fast computer graphics provides an exciting hands-on grasp of physics.

Microscopic particle simulations can most easily be related to the macroscopic descriptions of thermodynamics and hydrodynamics by using a particle description of macroscopic continuous matter. Continuum mechanics needs to be used because the short time and distance scales of molecular dynamics are too short and small for real-life problems. In continuum mechanics, the density, velocity, and energy are continuous functions of time and space.[2,3] The evolution of the continuous functions $\rho(r,t)$, $v(r,t)$, $e(r,t)$ is described by partial differential equations which include the gradients of the pressure tensor P and the heat flux vector Q:

$$\dot{\rho} = -\rho \nabla \cdot v, \quad (2a)$$

$$\rho \dot{v} = -\nabla \cdot P, \quad (2b)$$

$$\rho \dot{e} = -\nabla v : P - \nabla \cdot Q. \quad (2c)$$

The colon notation used here—consider $A:B$ as an example—indicates a tensor sum of all the terms of the form $A_{ij}B_{ij}$. There are four such terms for two-dimensional systems and nine for three-dimensional systems. A clever interpolation technique makes it possible to solve these continuum equations with a particle technique (smooth particle applied mechanics which closely resembles molecular dynamics (see Sec. VIII).

In the following we first consider two pedagogical one-dimensional problems, one equilibrium and one nonequilibrium. Then we illustrate the microscopic and the macroscopic particle techniques for a two-dimensional problem, the equilibration and collapse of a column of fluid exposed to a gravitational field. We also describe other applications for both fluids and solids. Although our example problems are given for one- or two-dimensional systems, the same techniques are easily applied in three dimensions. For references to many problems of this kind see Ref. 4.

II. OVERVIEW OF MOLECULAR DYNAMICS

One of the first applications of molecular dynamics was Vineyard's 1959 simulations[9] (see Fig. 1) of radiation damage in crystalline metals. His goal was to model real materials, such as copper, which were exposed to energetic radiation. Most of the other work until about 1980 focused instead on theoretical considerations, assessing the validity of statistical mechanics by obtaining the equation of state[14] and transport coefficients[15] from simple expressions for the temperature, pressure, and energy, along with the nonequilibrium currents described by Green and Kubo's linear response theory. By 1990 it was possible to simulate realistic systems with one million atoms.[16] Today simulations with many millions of atoms are routine and short simulations with billions

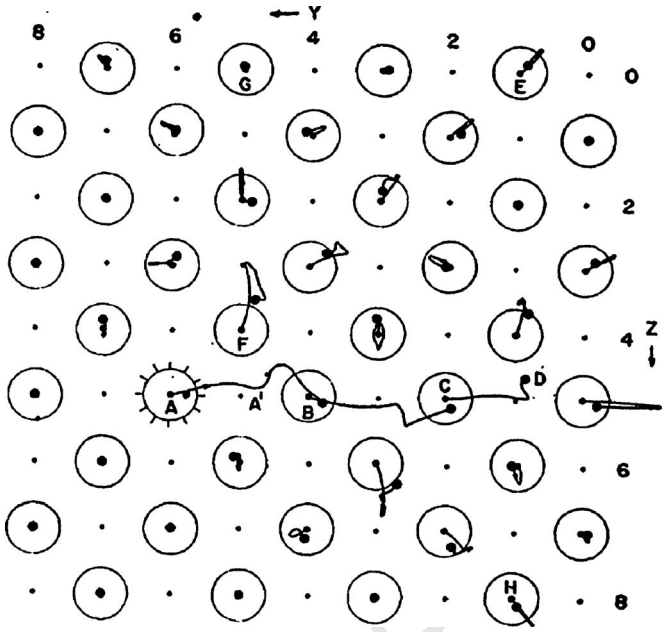

Fig. 1. Illustration of copper atom trajectories in Vineyard's 1959 simulation of radiation damage. The atom initially at "A" received an energy of 40 eV. Typical system size was 500 atoms (see Ref. 9).

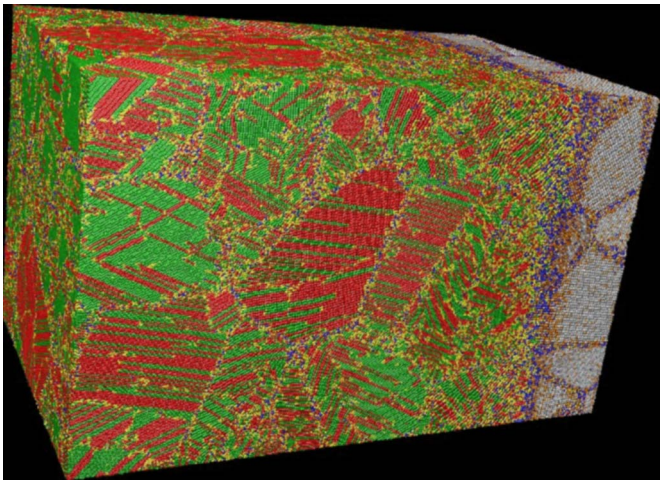

Fig. 2. Contemporary simulation of shockwave deformation. Typical system size was 30,000,000 atoms (see Refs. 7 and 8).

(thousands of millions) of atoms have been done on large scale weapons laboratory computers[7,8] (see Fig. 2).

Many problems today deal with systems away from equilibrium. Corresponding algorithmic formulations of boundary conditions such as prescribing the time dependence of the motion or stress and temperature or heat flow are essential ingredients of simulations of such nonequilibrium processes.[17] In the 1980s control theory began to be used to impose the kinetic temperature or pressure-tensor components by computational feedback of which the thermostated Nosé-Hoover equations of motion are an early example,[18,19]

$$m\ddot{r}_i = m\dot{v}_i = F_i - \zeta m v_i \tag{3a}$$

$$\dot{\zeta} = \left[\sum_{j=1}^{n} (m v_j^2 / kT_{\text{kinetic}}) - 1 \right] / n\tau^2, \tag{3b}$$

where n is the number of thermostated degrees of freedom. The equations of motion include a control variable ζ and are based on the kinetic theory definition of temperature in terms of the particle momenta p,

$$dkT_{\text{kinetic}} \equiv \langle mv^2 \rangle = \langle p^2/m \rangle \,. \quad \text{(d spatial dimensions)} \tag{4}$$

The kinetic temperature T_{kinetic} is the specified temperature for n thermostated degrees of freedom and τ is a relaxation time, which can generally be chosen based on physical grounds. The control variable ζ is the new aspect of the equations of motion. Note that the long-time average of its motion equation implies exact temperature control: $\langle \dot{\zeta} \rangle = 0$ implies $\langle mv^2 \rangle = kT_{\text{kinetic}}$. Here ζ controls the temperature. For any stationary state the time-averaged time derivative $\langle \dot{\zeta} \rangle$ necessarily vanishes. Analogous control variables have been developed to control stress and heat flux.[1,2]

By using two or more temperatures heat flow can be simulated, as we illustrate in Sec. IV. Thermostated equations of motion are required whenever it is necessary to extract the energy transferred associated with irreversible processes. The temperature kT_{kinetic} corresponds to the usual ideal gas thermometer of classical thermodynamics. Michael Grünwald and Christoph Dellago recently developed a clever implementation of the ideal gas thermometer,[20] surrounding a thermostated group of atoms by cells of ideal gas (a sufficiently large number of atoms with a Maxwell-Boltzmann velocity distribution) which interact only with the thermostated group and not with each other. The definition of pressure for a finite system, for example, a Lennard-Jones or embedded-atom cluster is not clearcut, due to the absence of an unambiguous definition of the volume.[20]

More recently Landau and Lifshitz' expression for the configurational temperature[21] has been used. The expression

$$kT_{\text{configurational}} = \langle F^2 \rangle / \langle \nabla^2 \mathcal{H} \rangle \tag{5}$$

appeared first as Eq. (33.14) of the 1951 Russian edition of their excellent text. Here $\mathcal{H}(q,p)$ is the Hamiltonian, from which the equations of motion for the coordinates q and momenta p can be derived. The definition Eq. (5) has been used to impose a *configurational temperature* on selected degrees of freedom. For a toy model of a single thermostated oscillator (with all the parameters and Boltzmann's constant k set equal to unity) the Nosé-Hoover kinetic-thermostat equations of motion, $\dot{q} = p$, $\dot{p} = -q - \zeta p$, and $\dot{\zeta} = p^2 - T_{\text{kinetic}}$, can be converted to the configurational-thermostat equations of motion,[22,23]

$$\dot{p} = -q, \tag{6a}$$

$$\dot{q} = p - \zeta q, \tag{6b}$$

$$\dot{\zeta} = \left(\frac{F^2}{\nabla^2 \mathcal{H}} \right) - T_{\text{configurational}} = q^2 - T_{\text{configurational}}, \tag{6c}$$

by making the simple substitutions:

$$q, p, \zeta, t, T_{\text{kinetic}} \rightarrow -p, -q, -\zeta, -t, T_{\text{configurational}}. \tag{7}$$

Either of these equivalent sets of equations of motion has a wide variety of solutions, some regular and some chaotic.[24]

Travis and Braga[22] first published the equations of motion in Eq. (6) for this configurational thermostat, though the

same equations appeared a few years earlier in Owen Jepps' unpublished Ph.D. thesis.[23] For the usual anharmonic interparticle forces the configurational thermostat equations, which involve both the nonlinear forces and their gradients, are somewhat stiffer than the kinetic ones. Because kinetic temperature has a simple physical interpretation, it seems likely that kinetic temperature will prove to be more useful than its configurational cousin. The usual reason advanced for considering the configurational rather than the kinetic temperature is that the system flow velocity might not be known. (And the kinetic temperature has to be defined and measured relative to that flow velocity.) But simple averaging techniques, illustrated here for the free expansion problem in Sec. V, make this argument relatively weak.

The main limitations of molecular dynamics are the small time scales, the small spatial scales, the uncertainty in formulating the forces, and the use of classical mechanics. The first two of these difficulties are insurmountable and motivate the use of continuum mechanics for mesoscopic and macroscopic problems (see Sec. VIII).

III. THE SIMPLEST PROBLEM, A ONE-DIMENSIONAL HARMONIC CHAIN

To develop a particle-based computer program, it is useful to begin with a problem having a known analytic solution. The simplest dynamics problem of this kind is a variant of Fermi's anharmonic chain studies.[5] It is the Newtonian motion of a nearest-neighbor harmonic chain, in which the motion of the ith particle responds to forces linear in the relative displacements of its neighbors:

$$m\ddot{x}_i = m\dot{v}_i = \kappa(x_{i+1} - x_i - d) + \kappa(x_{i-1} - x_i + d). \tag{8}$$

We choose units such the mass m, the force constant κ, and the equilibrium spacing of the springs d are all equal to unity. The coupled set of linear ordinary differential equations becomes:

$$\ddot{x}_i = x_{i+1} - 2x_i + x_{i-1}. \tag{9}$$

The simplest choice for boundary conditions are time-independent rigid boundaries, with

$$x_1 = 1, \quad x_N = Nd = N, \quad \dot{x}_1 = 0, \quad \dot{x}_N = 0, \tag{10}$$

or time-independent periodic boundaries, with $\ddot{x}_1 = x_N - N - 2x_1 + x_2$ and $\ddot{x}_N = x_1 + N - 2x_N + x_{N-1}$ replacing the accelerations $\ddot{x}_1$ and $\ddot{x}_N$ for particles 1 and N.

The initial conditions for the chain can be chosen to correspond to sine wave displacements or velocities with a wavelength λ. The corresponding exact solutions are periodic in both time and space, and illustrate the dispersion relation for the dependence of the oscillation frequency on the wavelength,

$$\omega = 2\sin(k/2), \tag{11}$$

with $k = 2\pi/\lambda$. For either periodic or rigid boundaries, the total energy of the chain,

$$E = \frac{\kappa}{2}\sum_{ij\ \text{pairs}} (|x_{ij}| - d)^2 + \frac{m}{2}\sum_{i=1}^{N} \dot{x}_i^2, \tag{12}$$

is constant. In a numerical solution the computed energy depends on the time step Δt used in the Runge-Kutta integrator. It is an interesting exercise, illustrated in Figs. 3 and 4, to determine the power law dependence of the total energy on the time step Δt. An analytic expression for such a Runge-Kutta solution can be related to the single oscillator case discussed in Ref. 2, Sec. 1.6.

We generally prefer the fourth-order Runge-Kutta integrator on the grounds of simplicity and ease of use. Some workers prefer one or another of the various Gear predictor-corrector integrators. These integrators require only a single force evaluation per time step, rather than four. A stimulating article by Berendsen and van Gunsteren[25] provides a readable introduction to the Gear integrators, along with numerical results for the harmonic oscillator problem. Like the Runge-Kutta integrators, the Gear integrators replace the single-time step solution of a differential equation with a low-order polynomial in the time step Δt. Away from equilibrium, with non-Hamiltonian equations of motion, the symplectic integrators[25,26] originated by Störmer[26] and appropriate to Hamiltonian mechanics cannot be used.

Because the Runge-Kutta trajectory and energy errors for this system are only a bit smaller (a factor of 2 in the coordinate error and an order of Δt in the energy error) the Gear approach saves computer time. Note that an expensive part of the computation, finding the interacting neighbors, needs to be done only once per time step for either method.

More complicated boundary conditions can provide interesting problems. A steadily moving boundary (such as $x_1 = 1 + t$) provides an unsteady wave resembling a shockwave. The initial condition, $\dot{x}_i = -1$, applied to all particles, together with the time-independent boundary condition, $x_i > 0$, illustrates the possibility of inelastic collisions, in which the total energy is conserved while the total momentum of the chain, $\Sigma\dot{x}$, is only partially reflected by the rigid wall at $x = 0$. In this case some of the kinetic energy of the chain is converted to internal vibrational energy. Similarly, pairs of chains can be made to collide with one another. To implement the inequalities $x_i > 0$ most simply any particle with x_i less than 0 at the

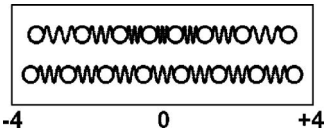

Fig. 3. A sinewave-displacement initial condition is shown, with the force-free chain illustrated below. The energy error incurred by the Runge-Kutta algorithm for this system is analyzed in Fig. 4.

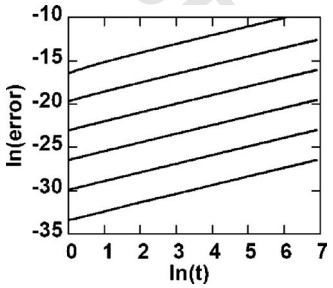

Fig. 4. Energy error as a function of time for $\Delta t = 0.01, 0.02, 0.04, 0.08, 0.16, 0.32$ for the eight-atom chain with an initial sinewave amplitude of 0.1. Fourth-order Runge-Kutta integration is used. The double logarithmic plot shows that the error at a fixed time varies as Δt^5, so that the single-step energy error is of order Δt^6.

end of a time step can be reflected from the rigid wall at $x=0$ by the pair of operations $x_i \to -x_i$ and $\dot{x}_i \to -\dot{x}_i$. Alternatively, a steep short-ranged repulsive potential can provide a reflector, as is illustrated in Eq. (25) of Sec. VI.

IV. KUSNEZOV AND AOKI'S ϕ^4 MODEL FOR HEAT FLOW

A slightly more sophisticated model than linear forces is required for a realistic treatment of heat flow. Such a model has been studied by Kusnezov and Aoki[27,28] in one, two, and three dimensions. It is remarkable that even the one-dimensional form of their ϕ^4 model illustrates Fourier's law for heat conduction. In addition to the harmonic nearest-neighbor spring forces the ϕ^4 model includes tethering forces,

$$\ddot{x}_i = -(x_i - i)^3, \tag{13}$$

which are derived from the tethering potential, $\phi = \frac{1}{4}(x_i - i)^4$. The latter localizes the particles near their lattice sites:

$$\langle x_i \rangle = i. \tag{14}$$

The localization provided by the tethers also furnishes sufficient anharmonicity for the chain to follow Fourier's law (as the chain becomes long and the temperature gradient becomes small):

$$\dot{T} = D_T \nabla^2 T \propto -D_T \nabla Q, \tag{15}$$

where Q is the heat flux vector, D_T is the thermal diffusivity, and $Q = -D_T \nabla T$. To study such problems requires a definition of the temperature T, either kinetic or configurational, as discussed in Sec. II. Endpoint kinetic temperatures can be constrained by using the Nosé-Hoover equations of motion,

$$\ddot{x}_1 = F_1 - \zeta_{\text{cold}} \dot{x}_1, \quad \dot{\zeta}_{\text{cold}} = \dot{x}_1^2 - T_{\text{cold}} \tag{16a}$$

$$\ddot{x}_N = F_N - \zeta_{\text{hot}} \dot{x}_N, \quad \dot{\zeta}_{\text{hot}} = \dot{x}_N^2 - T_{\text{hot}} \tag{16b}$$

for the endpoint particles, where F is the usual (nearest-neighbor plus tether) force, and the friction coefficients ζ (which can change sign as the motion progresses) control the average values of the endpoint particles temperatures. The endpoint particles can alternatively be thermostated with the configurational definition of T:

$$\dot{x} = v + \zeta F, \tag{17a}$$

$$\dot{v} = F, \tag{17b}$$

$$\dot{\zeta} \propto \frac{F^2}{kT_{\text{configurational}}} - \nabla^2 \mathcal{H}. \tag{17c}$$

Studies of these models[27,28] reveal an interesting dependence of the conductivity on the length of the chain and on the temperature gradient, $(T_{\text{hot}} - T_{\text{cold}})/(N-1)$ consistent with Fourier's law in the long chain limit. Figure 5 compares the long-time averaged temperature profiles obtained with both kinetic and configurational thermostats applied to just the first and last particles in the chain.

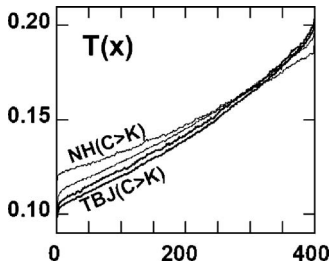

Fig. 5. Temperatures for a 400 particle ϕ^4 system. The first and last particles are thermostated (either Nosé-Hoover or Travis-Braga-Jepps thermostats are used) at temperatures of 0.1 and 0.2, respectively. At the cold end of the chain the configurational temperatures exceed the kinetic temperatures slightly for both these methods. In both simulations all the thermostat relaxation times τ were set equal to unity. Note that the abscissa is the particle number from 1 to 400.

V. IRREVERSIBLE FREE EXPANSION OF AN IDEAL GAS

The free expansion of a gas into a larger container is an interesting pedagogical problem. Thermodynamics gives an entropy increase of $Nk \ln(V_{\text{final}}/V_{\text{initial}})$ for this isoenergetic adiabatic process for an ideal gas, but Liouville's theorem states that the Gibbs' entropy, $-k\langle \ln f \rangle$, where f is the many-body phase-space probability density and a constant of the motion, is unchanged.

Simulation can give insight into this apparent paradox. Imagine, as an initial condition, a checkerboard array of squares, one fourth of which are occupied by a compressed ideal gas (density $\rho = 4$) with the rest of the squares empty. The subsequent motion equilibrates quickly, with an average density $\rho = 1$ in all the squares. Such an expansion can be modeled by using a "unit cell" of four squares, one full and three empty, with periodic boundary conditions. Snapshots from a simulation of this free expansion[29] for particles interacting with Lucy's short-range pair potential,[3,29]

$$\phi(r < h) = \frac{5}{\pi h^2}[1 - 6(r/h)^2 + 8(r/h)^3 - 3(r/h)^4], \tag{18}$$

are shown in Fig. 6. As explained in Sec. VIII, this functional form is the simplest twice-differentiable function vanishing at $r = h$ and having its maximum at $r = 0$. The constant $5/(\pi h^2)$ has been arbitrarily selected so as to satisfy the normalization condition appropriate to two dimensions

$$\int_0^h \phi(r) 2\pi r dr = 1. \tag{19}$$

Even in the absence of any hydrodynamic motion, Lucy's pair potential provides a reasonable model for an ideal gas. Although an ideal gas has only negligible interactions between particles, the Lucy potential of interaction leads to the same ideal-gas equation of state ($P \propto \rho^2$), as the virial theorem shows.[1,2,29]

The virial theorem for the potential contribution to the pressure involves the number density of particles separated by the distance r:

PROOF COPY 007803AJP

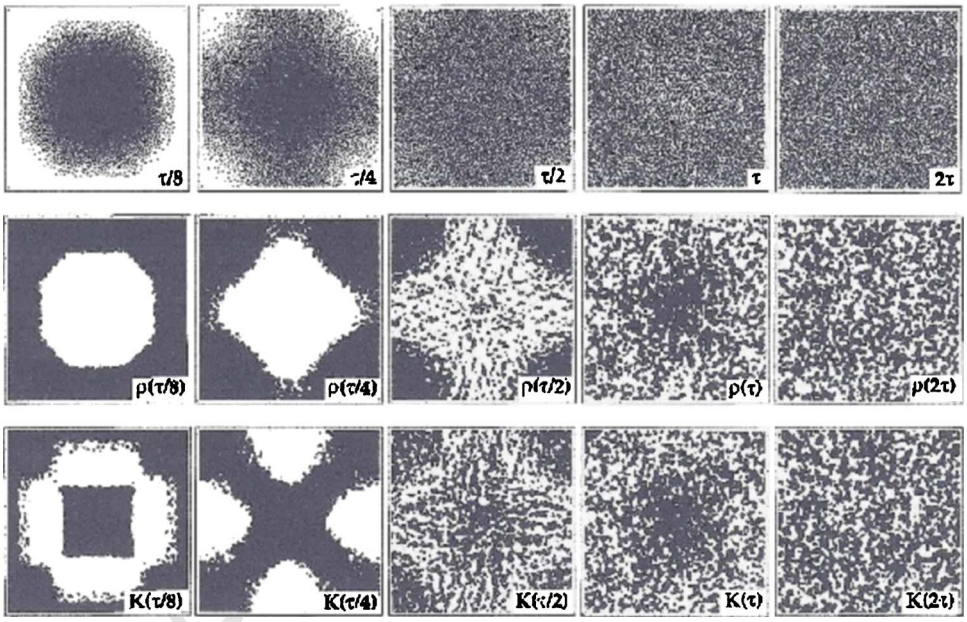

Fig. 6. Snapshots from a 16,384 particle free expansion in which the density decreases by a factor of 4. The average number of interacting neighbors varies from about $2\pi h^2 \approx 60$ to $\pi h^2/2 \approx 15$ as the motion develops. The range of the Lucy potential is $h=3$ and the particle mass is unity. The boundary separating the black and white region is the contour of average density/kinetic energy in the two contour plots. The total time interval shown corresponds to two sound-traversal times (see Ref. 29).

$$PV = \frac{1}{2}\sum F_i \cdot r_i = \frac{1}{2}\sum_{i<j} F_{ij} \cdot r_{ij}$$

$$= -\frac{N}{4}\int_0^\infty r\phi'(r)\rho(r)2\pi r dr. \tag{20}$$

For large enough h a random distribution of unit mass particles is appropriate: $\rho(r)=N/V$. In this case an integration by parts reproduces the ideal gas adiabatic equation of state:

$$PV = \frac{N}{2}\frac{N}{V}\int_0^h \phi(r)2\pi r dr = \frac{N}{2}\rho \rightarrow P = \frac{\rho^2}{2}. \tag{21}$$

A 16,384-particle simulation of the expansion is illustrated in Fig. 6. The equations are just those of ordinary molecular dynamics, but using the Lucy potential to represent the ideal-gas fluid. As the fluid expands, locally averaged values of the density, velocity, and kinetic energy can be calculated as weighted sums:

$$\rho(r) = \sum_i mw(r_i - r) \tag{22a}$$

$$\rho(r)v(r) = \sum_i mw(r_i - r)v_i \tag{22b}$$

$$\rho(r)e(r) = \sum_i mw(r_i - r)\frac{1}{2}v_i^2, \tag{22c}$$

where $w(r<h)$ is a normalized weight function with a sufficient range h to include several particles in the sums. A good choice for w has the same form as Lucy's potential, $w(r<h)=\phi(r<h)$ in Eq. (18). Such spatially weighted averages are the basis of smooth particle applied mechanics[3] as discussed in Sec. VIII.

Calculations of these field variables on a finely meshed grid provide a precise description of the continuum evolution. The average density and kinetic energy contours are the boundaries between the white and black portions of Fig. 6. Equilibration is rapid, with a nearly homogeneous fluid resulting after about two sound traversal times. An understanding of the actual entropy increase of the expansion, (computed in the usual way from the ideal gas equation of state) is shown in Fig. 7 for five system sizes, and despite Liouville's theorem, can be based on the thermal energy fluctuations, which is the part of the kinetic energy density over and above that associated with the flow, $\rho v^2/2$. In two spatial dimensions the relation is

$$2kT/m = \langle v^2 \rangle - \langle v \rangle^2. \tag{23}$$

It is necessary to subtract the flow velocity $\langle v \rangle$ from the particle velocities because temperature is measured in a *co-moving* frame, a coordinate frame moving along with the flow. The simple ideal gas thermodynamic formula $S/Nk = \ln(VT)$, where T is the thermal energy computed in this way, accounts nicely for the irreversible entropy increase associated with the free expansion.

VI. GRAVITATIONAL EQUILIBRATION AND COLLAPSE OF A FLUID COLUMN

A two-dimensional molecular dynamics simulation of the equilibration of a fluid column under the influence of gravity involves solving four first-order differential equations for each particle:

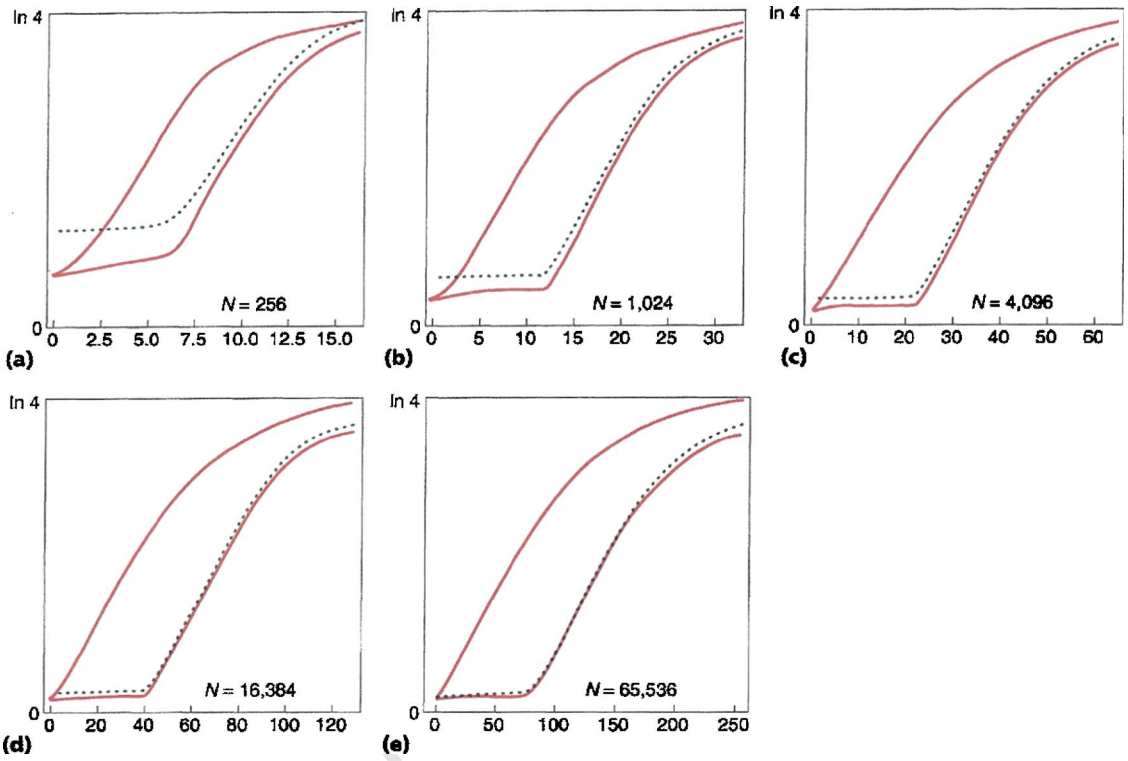

Fig. 7. Time dependence of the increase of entropy as a function of the number N of smooth particles used in the free expansion problem in Sec. V. The entropy calculated here is based on the thermal energy fluctuations described in that section. The lower curve and the dots indicate particle-based and cell-based entropies. A third "entropy," based on the total (in the fixed laboratory frame) thermal energy (the upper curves), incorrectly indicates an entropy increase even during the adiabatic expansion phase, and prior to the expanding fluid's impact with its periodic image. For each of the system sizes shown in the figure the ordinate scale varies from 0 to the expected entropy change, $\Delta S/Nk = \ln 4$. The abscissa is the elapsed time since the motion began, which varies from 0 to the sound-traversal time of the periodic box.

$$\dot{x} = p_x, \quad \dot{y} = p_y \tag{24a}$$

$$\dot{p}_x = F_x - \left(\frac{p_x}{\tau}\right), \quad \dot{p}_y = F_y - g - \left(\frac{p_y}{\tau}\right). \tag{24b}$$

To avoid complexity we have omitted the particle subscript i in these coordinate and momentum equations of motion for a typical particle. We have also chosen the particle mass equal to unity. Notice that the force in the y direction includes the gravitational acceleration $-g$ and that the frictional forces $-p/\tau$ remove heat with a characteristic time scale τ. A steep one-body repulsive potential,

$$\Phi_{\text{wall}} = \sum_i 50\delta y_i^4, \quad (\text{for } \delta y = y_i < 0), \tag{25}$$

provides a simple implementation of a perfectly reflecting boundary at the base of the column. A similar potential near the top of the column makes for a more efficient equilibration.

A close to correct initial condition for the column could be obtained by first solving the force-balance equations for the density $\rho(y)$:

$$\frac{dP}{dy} = \frac{\partial P}{\partial \rho}\frac{d\rho}{dy} = -\rho g, \tag{26}$$

and then choosing an initial square or triangular lattice spacing nonuniform in y and corresponding to this y-dependent density. Instead it is simpler to begin with a regular stress free lattice (such as a square or simple cubic lattice with the density chosen so that the total force on each particle vanishes) and to let the frictional forces $-p/\tau$ do the work of selecting the proper initial condition.

For simplicity, and to eliminate low-order numerical integration errors, we choose a very smooth and short-range pair potential, the difference of two simple polynomials, vanishing beyond $r=\sqrt{2}$, and with a maximum $\phi(r=0)=224$ and a minimum of $\phi(r=1)=-1$,

$$\phi(r < \sqrt{2}) = (2 - r^2)^8 - 2(2 - r^2)^4. \tag{27}$$

During the equilibration phase we additionally rescale the particle velocities at the end of every time step to impose a thermal energy equal to the well depth at the minimum,

$$\langle mv^2 \rangle = 2kT = 1. \tag{28}$$

Without this velocity rescaling the frictional forces would eventually remove all of the column's kinetic energy and force it to solidify. A time of order several sound traversal times is sufficient for the finite-temperature equilibration used here, after which the lateral periodic boundary is released so that the column can expand laterally and collapse.

Figure 8 shows snapshots from a 5000 particle simulation,[3] where the equilibrated height of the column (initially 100) is about 80 for a column width of 50. The subsequent collapse generates a lateral expansion, which occurs at a speed somewhat less than the speed of sound. We can

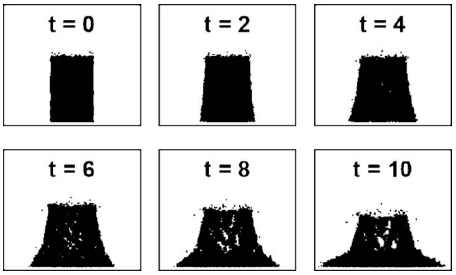

Fig. 8. Gravitational collapse of a pair-potential column. The equilibrated width is 50 and the equilibrated height is 80, both in units of the stress-free interparticle spacing. The total number of particles is 5000. The strength of the gravitational field $g=0.50$, as is the thermal energy kT. A viscous relaxation time $\tau=10$ was applied for a time interval $\Delta t=190$ using fourth-order Runge-Kutta with time step $\Delta t=0.01$. The time interval over which the collapse is illustrated is for the subsequent time interval $0<t<10$. Note the presence of tensile voids and some surface evaporation.

estimate the sound speed $c \approx 10$ for a triangular lattice with the interparticle spacing and the particle mass both equal to unity and with a stress-free density of $\sqrt{4/3}$:

$$c = \sqrt{\left(\frac{\partial P}{\partial \rho}\right)_{\rho=\sqrt{4/3}}} = \sqrt{96}. \tag{29}$$

After the vertical boundary constraints are released, tensile "rarefaction waves" move inward from the edges of the column, eventually leading to sufficiently negative pressure to cause the formation of internal voids. The kinetics and morphology of the void formation is an interesting and challenging subject. Particular solution details depend on the type and the range of the interparticle forces. We could, for instance, explore the consequences of a van der Waals' model by using a hard-core repulsive potential plus a longer-ranged attraction. A fundamental continuum treatment of the collapse process is also feasible. Such a treatment would involve formulating the dependence of the surface tension and viscosity on the local state variables, and the specification of a failure model leading to void formation. The irregular nature of the atomistic shape, for the system width shown here of 50 atoms motivates the study of this same problem using continuum mechanics. We do such a simulation with SPAM in Sec. X.

VII. CONTINUUM MECHANICS WITH FINITE ELEMENTS

Ever since computers became available, continuum problems of interest to engineers have been solved with finite-element methods.[30] In this approach each part of the structure or system being simulated is divided into small parts, "elements" defined by a grid of "nodes." In an Eulerian fixed-grid treatment the nodes are fixed in space, while a Lagrangian moving-grid method uses nodes which move with the underlying material. In either case the elements are generally chosen small enough that all the dependent variables (density, velocity, stress, energy density, …) can be approximated by simple polynomials within each element. In the equation of motion for the nodes it is usual to assume that the masses are lumped at the nodes. The time step in the finite-element simulations is limited by the smallest sound-traversal time among the elements. The gradients appearing in the continuum equations can then be averaged over the elements so as to formulate ordinary differential equations for the dynamics of the nodes. Much effort in the finite-element approach is devoted to generating suitable numerical meshes for the structure of interest.

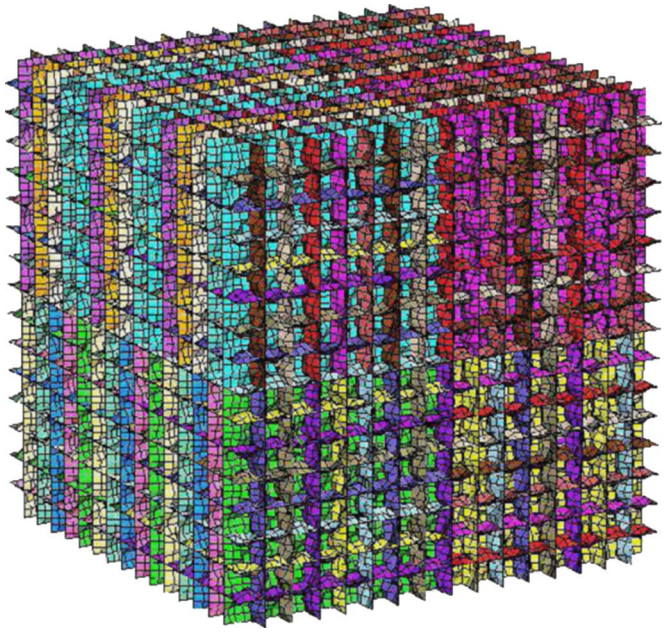

Fig. 9. Auxetic structure composed of 208,896 "shell" elements. The basic building blocks for this structure are 4×4 arrays of shell elements oriented perpendicular to the x,y,z coordinate directions.

Any well-posed continuum approach to materials simulation must solve the partial differential equations for the density, velocity, and internal energy $\rho(r,t)$, $v(r,t)$, $e(r,t)$ by formulating both the pressure tensor P and the heat flux vector Q in terms of the past and present values of ρ,v,e given in Eq. (2). In problems with external sources and sinks of momentum and energy (like gravity) corresponding terms are added to the right-hand sides of these conservation equations.

The simplest forms of the nonequilibrium parts of P and Q are Newton's and Fourier's laws for the dependence of the viscous stress on the velocity gradient and for the dependence of the heat flux vector on the temperature gradient. A continuum has an infinite number of degrees of freedom. A finite and regular grid, imposed on a continuum, can generate either Eulerian (if the grid is fixed) or Lagrangian (if the grid moves with the continuum) finite elements.

Relatively complex materials and structures can be built up of simple components, themselves composed of a few finite elements. Typical engineering applications model bridges, buildings, automobiles, and airplanes with finite-element descriptions. As a more microscopic example of a finite-element application in materials science, consider the mesoscopic structure of an auxetic material, a material with a negative value of Poisson's ratio. Such an odd material expands transversely when it is stretched, and shrinks when it is compressed. Simple structures composed of identical pores provide a useful model for this behavior. Figure 9 shows an auxetic material model[31] put together by connecting elastic-plastic finite elements to model a possible mesoscopic cell structure. Simulations, carried out by controlling the motion of the external surfaces of the model, confirm the auxetic behavior.[31]

VIII. CONTINUUM MECHANICS WITH PARTICLES [SPAM]

Because the microscopic time scale and length scale limits of atomistic dynamics make macroscopic atomistic simulations impossible, it is natural to seek alternative macroscopic particle methods. These resemble the finite-element methods we described in Sec. VII, but the polynomial representation is bypassed and is replaced by a simple particle sum. This method, which we call SPAM, which is described in the following, is simpler than the conventional Eulerian and Lagrangian finite-element methods, in that no shape functions and no integrations over elements are involved.

Eulerian interface and Lagrangian tangling are the main difficulties for finite elements. They can be avoided by using an irregular grid made up of moving particles. The interactions governing the particles' motion are determined by the constitutive properties of the continuum. This approach was conceived by Lucy and Monaghan.[32,33] They called it "sph" for "smooth particle hydrodynamics." Because this name suggests that the method only applies to fluids (and water in particular), we prefer the name "SPAM" (an acronym for Smooth Particle Applied Mechanics) to indicate its applicability to both fluid and solids, not just water.

Lucy and Monaghan visualized macroscopic (even astronomical!) chunks of material with individual masses, velocities, energies, pressure tensors, and heat-flux vectors. The spatial extent and range h of influence of each chunk is described by a smooth finite-range weighting function $w(r<h)$. The density at any point in space is computed by summing the contributions of all sufficiently near particles, as is also the local continuum value of F, an appropriate average of the smooth-particle values F_j:

$$\rho(r) = \sum_j m w(r_j - r) \tag{30a}$$

$$\rho(r) F(r) = \sum_j m F_j w(r_j - r) \tag{30b}$$

for $|r_j - r| < h$. Because the location r can be anywhere, not necessarily at a particle, this interpolation method makes it possible to interpolate field variables $F(r)$ onto any convenient grid, such as a square grid used to generate contour plots or Fourier transforms.

This smooth particle approach provides simple expressions for all the gradients. These expressions for the gradients are important because the right-hand sides of the continuum equations all involve such gradients, $\nabla\rho$, $\nabla\cdot P$, $\nabla\cdot Q$, ∇v, ∇T. For example, the continuity equation becomes equivalent to a set of ordinary differential equations (actually identities) for the particle densities:

$$\dot\rho = -\nabla\cdot(\rho v) + v\cdot\nabla\rho \tag{31a}$$

becomes

$$\dot\rho_i = -\sum_j m v_j\cdot\nabla_i w_{ij} + m v_i\cdot\sum_j \nabla_i w_{ij} = \sum_j m v_{ij}\cdot\nabla_i w_{ij}. \tag{31b}$$

Similarly, the equations of motion become ordinary differential equations for the particle velocities. That is,

$$\dot v = -\left(\frac{\nabla\cdot P}{\rho}\right) = -\nabla\cdot\left(\frac{P}{\rho}\right) - \left(\frac{P}{\rho^2}\right)\cdot\nabla\rho \tag{32a}$$

becomes

$$m\dot v_i = -\sum_j m^2[(P/\rho^2)_i + (P/\rho^2)_j]\cdot\nabla_i w_{ij}. \tag{32b}$$

Here the $v_{ij}=v_i-v_j$ are the relative velocities of nearby pairs of particles and the w_{ij} are the weight functions evaluated for the separation between particles i and j.

These ordinary differential equations conserve both the mass and the linear momentum exactly. The energy equation, which takes both heat and work into account, can likewise be written in a completely conservative way. We solve the complete set of continuum equations in Sec. IX for the Rayleigh-Bénard problem, which includes the need for specifying boundary velocities and temperatures.

In general, numerical solutions of the particle equations require both initial and boundary conditions.[3] The initial conditions include the initial arrangement and motion of all the particles. The boundary conditions typically involve specific algorithmic rules for the "collisions" of particles with surfaces[34] and for specific particle properties at or near surfaces. A relatively simple, but still challenging, example problem for continuum simulation is the free expansion of a gas, treated with atoms in Sec. V. Imagine an infinite checkerboard geometry with the initial condition that one-fourth of the cells are filled with motionless gas. Then, to start the dynamical motion, the particles are allowed to move. As the dynamics develops, rarefaction waves converge on the center of the filled cells while shockwaves form when gases from next-neighbor cells collide. The singular nature of this problem causes difficulty for either Eulerian or Lagrangian finite-element codes.[29]

The smooth-particle approach is quite different. Using the ideal gas adiabatic equation of state $P=\frac{1}{2}\rho^2$ and choosing the particle mass m equal to unity, the smooth-particle motion equations become

$$\dot v_i = -\sum_j \nabla_i w_{ij}, \tag{33}$$

so that the continuum dynamics corresponds precisely to the atomistic development of the fluid illustrated in Sec. V. The effective pair potential w is the smooth-particle weight function, with range $r<h$. The simplest choice for the weight function is a polynomial, with a maximum at $r=0$ and which vanishes, along with two vanishing derivatives at $r=h$. As before, the form is the same as given in Eq. (18). This weight function, the choice originally proposed by Lucy in 1977,[32] was used in the free expansion simulation illustrated in Fig. 6, which shows both the particles and the contours of the average density and kinetic temperature for times up to two sound traversal times. It is clear that a particle method is ideal for such complicated flow problems.

This free expansion problem underscores the importance of proper interfacial boundary conditions. When fluids collide, some mechanism must act to prevent their interpenetration. To avoid the interpenetration of oppositely directed gases a modification of the straightforward smooth-particle approach, due to Monaghan,[35] can be used. Monaghan replaced the usual velocity definitions, $\dot r_i = v_i$, with

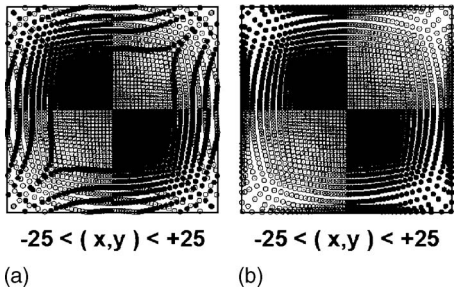

Fig. 10. Late time distribution of smooth particles using (a) the usual velocity definition, $\dot{r}=v$, and (b) Monaghan's modified velocity as given in Eq. (34). Notice that the mixing of particles from adjacent quadrants shown at the left is avoided by Monaghan's motion equations.

$$\dot{r}_i = v_i + m\sum_j [v_j - v_i](w_{ij}/\rho_{ij}), \tag{34}$$

where ρ_{ij} is either the arithmetic or the geometric mean of the densities at particle i and particle j. Summing Monaghan's velocity definition over all particles gives exact conservation of momentum because the relative velocity sum vanishes by symmetry:

$$m\sum_i \sum_j [v_j - v_i]w_{ij}/\rho_{ij} = 0. \tag{35}$$

It is easy to confirm that this approach also conserves the mass and momentum exactly. Figure 10 shows the improved interface behavior using Monaghan's approach.[35]

IX. RAYLEIGH–BÉNARD CONVECTION WITH SMOOTH PARTICLES

An interesting problem with relatively simple time-independent boundaries is the behavior of a compressible fluid in a gravitational field. For such a fluid, heated from below and cooled above, heat can be transferred upward by either of two mechanisms. If the temperature gradient is sufficiently small, motionless Fourier conduction results. If the temperature gradient exceeds a certain threshold, steady convective rolls form, and the heat transfer becomes convective. At still higher temperature gradients complex turbulent flows can result.[3] This problem is ideal for students. An interesting aspect of the numerical solutions using particles is that with too few particles the smooth-particle fluid can freeze, preventing the formation of convective rolls. Figure 11 illustrates the flow using Lucy's weight function for 5000 smooth particles. Here the Rayleigh number,

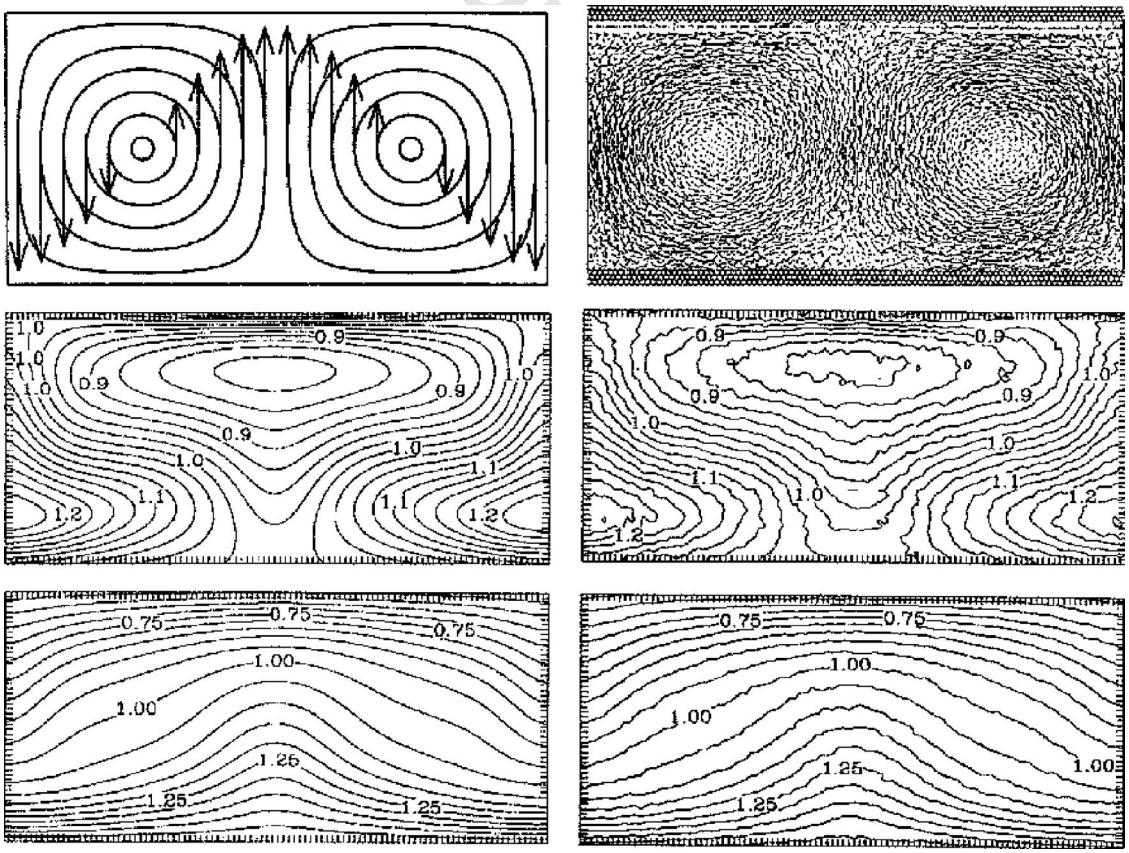

Fig. 11. Rayleigh-Bénard simulation. The initial velocities are shown at the top left with a late-time smooth-particle snapshot at the top right. Convection in a gravitational field with periodic lateral boundaries and mirror-image boundaries at the top and bottom imposes a Rayleigh number $R=10000$ on the ideal-gas fluid with constant transport coefficients. A comparison of Rayleigh-Bénard densities and energies as computed with exact continuum mechanics (left) and SPAM particles (right), appears in the bottom two rows (see Ref. 34).

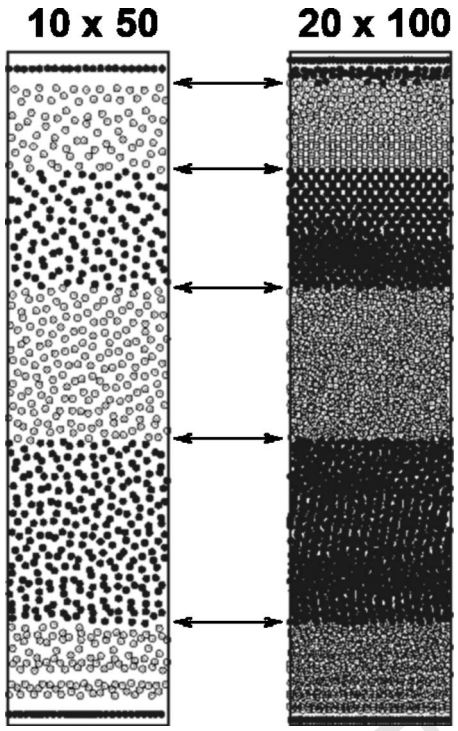

Fig. 12. Equilibrated particle distributions for 500 and 2000 smooth particles, with a reflecting boundary at $y=0$ and periodic boundaries at $x=\pm L/2$. The particles have been shaded to indicate equally spaced density contours. The arrows indicate the corresponding exact contour locations from an exact continuum calculation.

$$R = \frac{gH^4(\Delta T/H)}{\nu D_T} = 10000, \tag{36}$$

is large enough that the particles provide a realistic description of the continuum flow field. Here g is the gravitational field strength, H is the system height, ΔT is the top-to-bottom temperature difference across the system, ν is the kinematic viscosity $\nu=\eta/\rho$, and D_T is the thermal diffusivity. The flow shown in Fig. 11 corresponds to an ideal gas with constant transport coefficients, described in Ref. 36. Figure 11 compares the approximate smooth-particle solution to the exact solution of the continuum flow equations.

The boundary conditions for the Rayleigh-Bénard problem have to specify the velocity and the temperature at the top and bottom of the fluid. In the flow illustrated in Fig. 11 the lateral boundaries are periodic. The top and bottom boundary conditions are implemented by introducing "ghost" or "image" particles outside the system in such a way that averages which include these extra particles exactly satisfy the desired boundary conditions.

X. GRAVITATIONAL COLLAPSE OF A CONTINUUM COLUMN USING SPAM

In Sec. VI we considered the equilibration and collapse of a column using molecular dynamics. Here we consider the continuum analog of this problem using SPAM. We use the simple polynomial equation of state:

$$P = (\rho/\bar{\rho})^3 - (\rho/\bar{\rho})^2 = \rho^3 - \rho^2, \tag{37}$$

where $\bar{\rho}=1$ is the stress-free equilibrium density. For simplicity, we set both the particle mass and the stress-free density equal to unity here. The SPAM particle densities are calculated as usual, using Lucy's form of the weighting function in Eq. (18). For simplicity here we choose the mass of each particle equal to unity, so that the mass density and the number density are equal. Notice that the integral of the weight function over space,

$$\int_0^h w(r) 2\pi r dr = 1, \tag{38}$$

is unity, so that a completely random distribution of N particles in a volume V, with the average number density $\bar{n}=N/V=\bar{\rho}/m=1$ and average mass density $\bar{\rho}=Nm/V=\bar{n}m=1$, provided that h is sufficiently large, gives

$$\langle n\rangle = \frac{1}{N}\sum_i \sum_j w_{ij}, \quad \langle \rho\rangle = \frac{1}{N}\sum_i \sum_j m w_{ij}. \tag{39}$$

The smooth-particle equations of motion take the form,

$$m\dot{v}_i = -\sum_j m^2[(P/\rho^2)_i + (P/\rho^2)_j]\cdot\nabla_i w_{ij}. \tag{40}$$

If we use the polynomial equation of state

$$P/\rho^2 = (\rho/\bar{\rho}^3) - (1/\bar{\rho}^2) = \rho - 1, \tag{41}$$

we obtain

$$\begin{aligned} m\dot{v}_i &= -\sum [(\rho_i-\bar{\rho})\nabla_i(\rho_i) + (\rho_j-\bar{\rho})\nabla_i(\rho_j)] \\ &= -\sum [\rho_i + \rho_j - 2]\nabla_i w(r_{ij}). \end{aligned} \tag{42}$$

The fourth-order Runge-Kutta solution of these equations of motion conserves energy apart from a small single-step error of order Δt^6. (There is also a phase error of order Δt^5 which does not affect the energy.) The SPAM equations of motion are equivalent to those computed in molecular dynamics from a many-body potential function designed to minimize density fluctuations:

$$\Phi = \sum_i \phi_i(\rho) = \sum_i \frac{(\rho_i - 1)^2}{2}. \tag{43}$$

In either interpretation the particle and mass densities ρ_i are simple sums: $\rho_i=\Sigma_j m w(r_{ij})$. The density at particle i is the sum of contributions of nearby particles that are within the maximum range h of the weighting function $w(r)$.

Although the SPAM motion equations induce a density near unity for each particle, the model contains no intrinsic surface tension. To model realistic flows with surfaces requires either the addition of a pair potential discouraging surface formation or the addition of a phenomenological surface-energy potential which minimizes density gradients,

$$\Phi_{\text{surface}} \propto \sum_{i=1}^{N} (\nabla_i \rho)^2. \tag{44}$$

Here we choose to use a surface potential with a proportionality constant of $1/10$.

For the density-dependent equation of state designed to give a density of unity at zero pressure, $P=\rho^3-\rho^2$, there is an additional unphysical feature. The SPAM particles tend to form one-dimensional chains or "strings." This undesirable chain formation can be overcome by using a very short-range core potential,

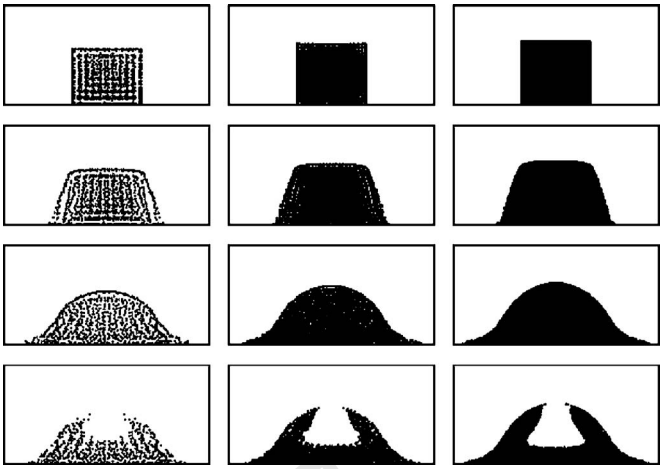

Fig. 13. Two successive stages of collapse of square equilibrated columns modeled by SPAM. Simulations with 640, 2560, and 10240 particles are compared at corresponding times. The bottom row indicates the regions of positive pressure. These results are taken from Ref. 3.

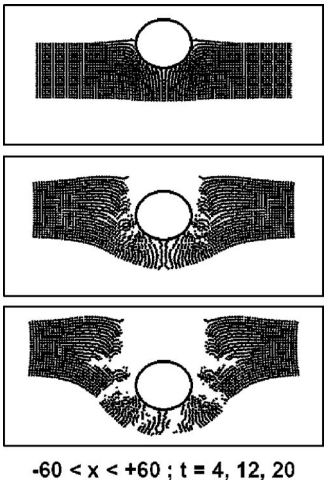

Fig. 14. Penetration of a plate by a ball using smooth particles. The interaction between the (rigid) ball and the particles making up the plate was modeled by a purely repulsive short-ranged pair potential.

$$\Phi_{\text{core}}(r<\sigma) \propto \sum_{i<j} (\sigma^2 - r^2)^4. \tag{45}$$

We choose a proportionality constant of unity and a core size $\sigma=0.6$.

Now consider the equilibration and collapse of a column of particles in a gravitational field g induced by the gravitational potential $\Phi_{\text{grav}}=\Sigma_i g y_i$. By imposing frictional forces, $F_{\text{friction}}=-p/\tau$ and appropriate boundary conditions, a stationary equilibrated structure can be obtained. Figure 12 corresponds to a field strength g chosen to give a structure with an overall density of 8/5 and an aspect ratio of five. The boundary condition at the bottom, $y>0$, is implemented by reflecting any particle violating that condition. That is, if $y_i<0$ we take $y_i \to -y_i$ and $\dot{y}_i \to -\dot{y}_i$. A comparison of the theoretical density profile with that computed in this way is shown in Fig. 12. Figure 13 shows the tensile regions formed in the collapse of square equilibrated columns, as given by the smooth-particle equations of motion.

XI. CONCLUSIONS

The problems we have illustrated barely scratch the surface of interesting applications from which new physics can be gleaned. In Ref. 3 we discuss several interesting problem areas, including the deformation of sea ice and the breakup of stellar clusters. Problems involving failure are a natural application of smooth-particle techniques. A failure model based on stress, strain, or energy can be implemented easily in a smooth-particle code. By comparing smooth particle simulations with laboratory experiments or with molecular dynamics simulations, it should be possible to develop useful predictive models of tensile and shear failure. The main difficulty and a good research area is the identification and elimination of the various instabilities that can arise in the presence of tensile stresses.

The penetration of a continuum by a projectile is a generic failure problem type with many applications. Figure 14 shows the progress of a round ball fired at an elastic-plastic plate. In treating such problems not only failure models, but also boundary conditions at material interfaces, are in need of development. The problem areas and solution techniques are mainly limited by our imagination, now that the cost of high speed computation is affordable.

A further advantage of the smooth particle approach, beyond the simplicity of ordinary differential equations, is the ease with which interpolation and rezoning can be carried out. If more detail is desired in a particular region, it is straightforward to include more particles there, maintaining the overall mass, momentum, and energy. Likewise, particles can be combined in more quiescent regions, saving computational effort.

ACKNOWLEDGMENTS

We thank Kris Wojciechowski for suggesting and encouraging us to contribute to the theme issue. We also thank Owen Jepps, Debra Searles, and Karl Travis for their help in establishing the chronology of the configurational temperature algorithms. Karl kindly read through the first draft of this manuscript and made several useful comments, as did the two referees.

[a]Electronic mail: hooverwilliam@yahoo.com

[1] Wm. G. Hoover, *Molecular Dynamics* (Springer-Verlag, Berlin, 1986).
[2] Wm. G. Hoover, *Computational Statistical Mechanics* (Elsevier, Amsterdam, 1991).
[3] Wm. G. Hoover, *Smooth Particle Applied Mechanics* (World Scientific, Singapore, 2006).
[4] Information about molecular dynamics and Refs. 1 and 2 is available at ⟨williamhoover.info⟩.
[5] J. L. Tuck and M. T. Menzel, "The superperiod of the nonlinear weighted string (Fermi Pasta Ulam problem)," Adv. Math. **9**, 399–407 (1972).
[6] B. J. Alder and T. E. Wainwright, "Molecules in motion," Sci. Am. **201**(4), 113–130 (1959).
[7] K. Kadau, T. C. Germann, and P. S. Lomdahl, "Molecular dynamics comes of age: 320 billion atom simulation on BlueGene/L," Int. J. Mod. Phys. C **17**, 1755–1761 (2006).
[8] K. Kadau, T. C. Germann, P. S. Lomdahl, R. C. Albers, J. S. Wark, A. Higginbotham, and B. L. Holian, "Shockwaves in polycrystalline iron," Phys. Rev. Lett. **98**, 135701-1–4 (2007).
[9] J. B. Gibson, A. N. Goland, M. Milgram, and G. H. Vineyard, "Dynamics of radiation damage," Phys. Rev. **120**, 1229–1253 (1960).
[10] A. J. C. Ladd and L. V. Woodcock, "Interfacial and coexistence properties of the Lennard-Jones system at the triple point," Mol. Phys. **36**, 611–619 (1978).

[11] T. Watanabe and H. Kaburaki, "Particle simulation of three-dimensional convection patterns in a Rayleigh-Bénard system," Phys. Rev. E **56**, 1218–1221 (1997).
[12] B. L. Holian, "Atomistic computer simulations of shockwaves," Shock Waves **5**, 149–157 (1995).
[13] I. M. Svishchev and P. G. Kusalik, "Crystallization of liquid water in a molecular dynamics simulation," Phys. Rev. Lett. **73**, 975–979 (1994).
[14] B. J. Alder and T. E. Wainwright, "Phase transition in elastic disks," Phys. Rev. **127**, 359–361 (1962).
[15] D. Levesque, L. Verlet, and J. Kürkijarvi, "Computer 'experiments' on classical fluids. IV. Transport properties and time correlation functions of the Lennard-Jones liquid near its triple point," Phys. Rev. A **7**, 1690–1700 (1973).
[16] W. G. Hoover, A. J. De Groot, C. G. Hoover, I. F. Stowers, T. Kawai, B. L. Holian, T. Boku, S. Ihara, and J. Belak, "Large-scale elastic-plastic indentation simulations via nonequilibrium molecular dynamics," Phys. Rev. A **42**, 5844–5853 (1990).
[17] W. G. Hoover, A. J. C. Ladd, and R. B. Hickman, "Bulk viscosity via nonequilibrium and equilibrium molecular dynamics," Phys. Rev. A **21**, 1756–1760 (1980).
[18] S. Nosé, "Constant temperature molecular dynamics methods," Prog. Theor. Phys. Suppl. **103**, 1–46 (1991).
[19] W. G. Hoover, "Canonical dynamics: Equilibrium phase-space distributions," Phys. Rev. A **31**, 1695–1697 (1985).
[20] M. Grünwald and C. Dellago, "Ideal gas pressure bath: A method for applying hydrostatic pressure in the computer simulation of nanoparticles," Mol. Phys. **104**, 3709–3715 (2006).
[21] L. D. Landau and E. M. Lifshitz, *Statistical Physics* (Pergamon Press, Oxford, 1980).
[22] C. Braga and K. P. Travis, "Configurational temperature Nosé-Hoover thermostat," J. Chem. Phys. **123**, 134101-1–15 (2005).
[23] O. G. Jepps, "The thermodynamic temperature in statistical mechanics," Ph. D. thesis, Australian National University, Canberra (2001).
[24] H. A. Posch, W. G. Hoover, and F. J. Vesely, "Canonical dynamics of the Nosé oscillator: Stability, order, and chaos," Phys. Rev. A **33**, 4253–4265 (1986).
[25] H. J. C. Berendsen and W. F. van Gunsteren, "Practical algorithms for dynamics simulations," in *Molecular Dynamics Simulation of Statistical Mechanical Systems*, edited by G. P. F. Ciccotti and Wm. G. Hoover (North-Holland, Amsterdam, 1986), pp. 43–65.
[26] G. D. Venneri and W. G. Hoover, "Simple exact test for well-known molecular dynamics algorithms," J. Comp. Phys. **73**, 468–475 (1987).
[27] K. Aoki and D. Kusnezov, "Nonequilibrium steady states and transport in the classical lattice ϕ^4 theory," Phys. Lett. B **477**, 348–354 (2000).
[28] Wm. G. Hoover, K. Aoki, C. Hoover, and S. de Groot, "Time-reversible deterministic thermostats," Physica D **187**, 253–267 (2004).
[29] Wm. G. Hoover, H. A. Posch, V. M. Castillo, and C. G. Hoover, "Computer simulation of irreversible expansions via molecular dynamics, smooth particle applied mechanics, Eulerian, and Lagrangian continuum mechanics," J. Stat. Phys. **100**, 313–326 (2000).
[30] O. C. Zienkiewicz, *The Finite Element Method in Engineering Science* (McGraw-Hill, London, 1971).
[31] Wm. G. Hoover and C. G. Hoover, "Searching for auxetics with DYNA3D and ParaDyn," Phys. Status Solidi B **242**, 585–594 (2005).
[32] L. B. Lucy, "A numerical approach to the testing of the fission hypothesis," Astron. J. **82**, 1013–1024 (1977).
[33] R. A. Gingold and J. J. Monaghan, "Smoothed particle hydrodynamics: Theory and application to nonspherical stars," Mon. Not. R. Astron. Soc. **181**, 375–389 (1977).
[34] O. Kum, Wm. G. Hoover, and C. G. Hoover, "Smooth-particle boundary conditions," Phys. Rev. E **68**, 017701-1–4 (2003).
[35] J. J. Monaghan, "On the problem of penetration in particle methods," J. Comp. Phys. **82**, 1–15 (1989).
[36] O. Kum, Wm. G. Hoover, and H. A. Posch, "Viscous conducting flows with smooth-particle applied mechanics," Phys. Rev. E **52**, 4899–4908 (1995).